Cavity Cooling Using Ultrafast Electrons

D. E. Maison,* L. Stettiner,* S. Even-Haim, A. Gorlach, and I. Kaminer†
Technion—Israel Institute of Technology, Haifa 3200003, Israel

(Received 14 April 2025; accepted 8 October 2025; published 14 November 2025)

We propose a method to cool a thermal photonic state in a cavity by passing electrons through it. Electrons are coherently split into two paths, with one path traversing the cavity, becoming entangled with its photonic state. A sequence of such entanglement interactions can achieve cooling of the cavity, e.g., a twofold reduction in thermal photon number with a 25% postselection probability. This "which-path" based approach extends to other qubit-oscillator systems, such as phonons in crystals or optomechanical resonators, offering a general framework for quantum oscillator cooling.

DOI: 10.1103/fnhk-lknl

Introduction—The interaction between electromagnetic fields and electrons is a cornerstone of modern electrodynamics. Since the explanation of the photoelectric effect a century ago, this field has continued to captivate researchers, particularly in the study of optical near-field interactions with free electrons [1–8]. These interactions provide a platform for probing the quantum properties of light [9–12]. For instance, Ref. [13] shows that energy-shaped free electrons in an optical cavity can generate nonclassical light states such as cat states [14,15] and Gottesman-Kitaev-Preskill states [16], which are crucial for quantum error correction [17–20]. Such studies are part of free-electron quantum optics [10,13,21–23], facilitating the electron-photon and electron-electron interactions for spectroscopy and microscopy [12,24,25], quantum light sources [13,26], and quantum information processing [27]. In all of these cases, electrons act as unique flying qubits, performing strong ultrafast interactions.

A key bottleneck for these prospects is achieving strong electron-photon interactions [28–33]. The leading schemes involve photonic cavity designs at various frequencies [6,30,34,35]. At low frequencies, relevant for most electron technologies, the quantum features of the interaction are highly temperature-sensitive. Key phenomena, such as electron-photon entanglement [10], require cooling the cavity close to the vacuum state. More broadly, for many quantum technologies, thermal decoherence at finite temperatures hinders state control [36–38]. Thermal photons obstruct high-fidelity quantum operations [39], reducing purity and coherence [40].

We propose cooling photonic modes via free-electron interactions with photonic structures. This represents a specific instance of quantum measurement-induced thermodynamic control [41]. Our scheme uses electron-photon interactions to implement a conditional displacement operator, enabling cavity cooling. While established feedback-based methods rely on real-time measurement and active control to manipulate the cavity state [42], our approach achieves cooling via interference without the need for active feedback. It can also direct a feed-forward scheme by altering consequent electrons. In this sense, our method resembles the measurement-induced state creation technique [43], introducing a probabilistic element. We analyze the cooling efficiency and the corresponding postselection probability as functions of interaction parameters and cavity properties.

Our free-electron cooling scheme can be viewed as a many-body "which-path" experiment [25] with the cavity acting as a detector. For optical cavities or other nanophotonic structures, the electron-photon interaction can be realized via photon-induced near-field electron microscopy [1] in transmission electron microscopes, a rapidly developing field with expanding capabilities [4,6,7]. The which-path cooling approach is not limited to cavities, but also applies to phonons and photonic quasiparticles in solids [44,45], and vibrational and rotational excitations in molecules [46]. This concept can also be extended to energetic particles beyond electrons, such as x-ray photons or neutrons [47,48].

Results—A quantum harmonic oscillator in a thermal state can be described by the following density matrix [49]:

$$\rho_{\bar{n}} = \frac{1}{\bar{n}+1}\sum_{n=0}^{\infty}\left(\frac{\bar{n}}{\bar{n}+1}\right)^{n}|n\rangle\langle n|, \tag{1}$$

where $\bar{n} = (\exp(\hbar\omega/kT)-1)^{-1}$ is the average number of thermal photons, ω is the oscillator frequency, T the temperature, and $|n\rangle$ the n-particle Fock state. Our goal is to reduce $\bar{n}$, thus lowering the temperature.

Alternatively, a quantum state can be described by the Wigner function [50], a quasiprobability distribution in the

*These authors contributed equally to this work.
†Contact author: kaminer@technion.ac.il

phase space. For the thermal state $\rho_{\bar{n}}$, it reads [51] as follows:

$$W_{\bar{n}}(x,p) = \frac{1}{\pi(2\bar{n}+1)} \exp\left(-\frac{x^2+p^2}{2\bar{n}+1}\right). \tag{2}$$

Here, x and p are dimensionless position and momentum quadratures. The thermal Wigner function is a symmetric origin-centered Gaussian, similar to the vacuum Wigner function $W_0(x,p) = W_{\bar{n}=0}(x,p)$, but with larger variances in both x and p. Because of the absence of a defined phase for a thermal state, its photon number cannot be reduced by regular displacement operations.

A system coupled to a bath thermalizes according to the Lindblad equation [52], which for an oscillator reads

$$\dot{\rho} = \frac{\kappa}{2}(n_b+1)(2a\rho a^\dagger - a^\dagger a\rho - \rho a^\dagger a) + \frac{\kappa}{2} n_b (2a^\dagger \rho a - a a^\dagger \rho - \rho a a^\dagger), \tag{3}$$

where κ is the dissipation rate, n_b is the bath photon number, a and $a^\dagger$ are the annihilation and creation operators. Thermalization brings the system to its thermal equilibrium, i.e., for $t \gg \kappa^{-1}$, the state converges to (1) with $\bar{n} = n_b$, independent of the initial state [52–54].

Our cooling scheme relies on free-electron interactions with photonic structures in a transmission electron microscope [2,3,10]. We consider microwave cavities, where the photonic mode frequency ω is much lower than the electron energy uncertainty. The scattering matrix for the electron-cavity interaction is the displacement operator [10,14,21],

$$D(g_Q) = \exp\left(g_Q a^\dagger - g_Q^* a\right). \tag{4}$$

It shifts the oscillator state in phase space (equivalent to shifting a classical field), acting on the Wigner function as $W_{D(g_Q)|\psi\rangle}(x,p) = W_{|\psi\rangle}(x - \sqrt{2}\Re g_Q, p - \sqrt{2}\Im g_Q)$ [14]. The interaction parameter g_Q characterizes the coupling strength between the electron and the cavity [2,3,10].

We propose a cavity cooling method based on electron interference and postselection. Similar to the iconic which-path experiment, electrons are first split into two paths, as in split-illumination holography [55]. We label the electron's left (right) path as $|0\rangle$ ($|1\rangle$), so that before passing through the cavity, the electron state is $|+\rangle = (|0\rangle + |1\rangle)/\sqrt{2}$. The cavity is placed along one path (the right path in this setup), as illustrated in Fig. 1. The scattering matrix then changes from the displacement operator (4) to the conditional displacement (CD),

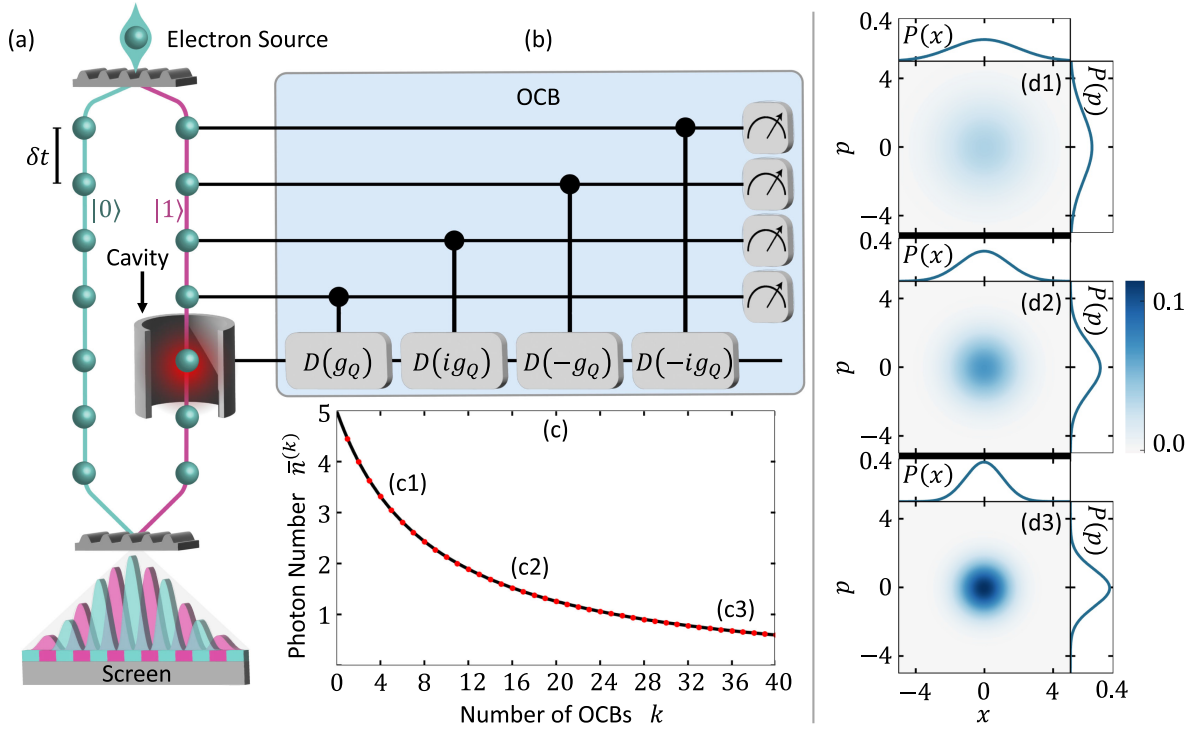

FIG. 1. Cavity cooling via free-electron interactions. (a) Electrons pass through a beam splitter with time interval δt and are split into two paths. The right path ($|1\rangle$) interacts with the cavity. The electron is measured in the $|\pm\rangle$ basis by observing where it hits the screen relative to the fringes of the interference pattern. (b) Equivalent quantum circuit of one cooling cycle illustrated as a single oscillator cooling block (OCB). (c) Number of thermal photons $\bar{n}^{(k)}$ as a function of the number of OCB iterations k. The initial state is thermal with $\bar{n}^{(0)} = 5$, and the electron-cavity interaction parameter is set to $g_Q = 0.1$. (d1)–(d3) Wigner functions of the states (c1)–(c3) after 4, 16, and 36 OCB iterations, respectively, as functions of quadratures x and p.

$$CD(g_Q) = |0\rangle\langle 0|\mathbb{1} + |1\rangle\langle 1|D(g_Q). \tag{5}$$

The projectors $|0\rangle\langle 0|$ and $|1\rangle\langle 1|$ operate on the electron state, while $\mathbb{1}$ and $D(g_Q)$ act on the cavity. CD can be thought of as a continuous-variable analog of the CNOT gate [56]: it shifts the photonic state when the electron state is $|1\rangle$, and acts as identity otherwise. Thus, it entangles the electron and the cavity, and, like CNOT, enables universal control in the joint Hilbert space [57].

The adjoint circuit in Fig. 1(b) "translates" the electron-cavity interaction into the quantum-gate framework. It combines continuous- and discrete-variable quantum information processes, with displacement operators acting on the oscillator (cavity), controlled by the qubits (electrons). Four consecutive CD operators form an "oscillator cooling block" (OCB), which can be repeated to improve the cooling efficiency.

The electron state after interaction is determined via its interference pattern [25]. Detecting the electron at an even (odd) fringe corresponds to the measurement outcome $|+\rangle$ ($|-\rangle$). Measuring the electron in the $|\pm\rangle$ basis is equivalent to applying the following Kraus operator to the photonic mode [58]:

$$\langle \pm|CD(g_Q)|+\rangle = D_{\pm}(g_Q) = \frac{1}{2}(\mathbb{1} \pm D(g_Q)), \tag{6}$$

with the mean value taken over the electron state (path). For a detailed discussion of Kraus operators in the context of projective measurements, see Ref. [59].

Following the "sharpen" method from Ref. [43], we apply the sequence $CD(-ig_Q)CD(-g_Q)CD(ig_Q)CD(g_Q)$ to cool the cavity state. After each CD, the electron is measured and postselected in the $|+\rangle$ state (see Fig. S1 in Supplemental Material [60]). When the heat exchange with the bath is negligible ($\kappa = 0$), the OCB can be represented as a product of Kraus operators (6),

$$D_{\mathrm{OCB}}(g_Q) = D_+(-ig_Q)D_+(-g_Q)D_+(ig_Q)D_+(g_Q). \tag{7}$$

If $|g_Q| \ll 1$, the operator D_{OCB} causes a photon number decrease—also applying to photonic states beyond thermal. Specifically, let the initial state be ρ. After D_{OCB}, the state is $\rho' = \mathcal{N} D_{\mathrm{OCB}}(g_Q)\rho D^{\dagger}_{\mathrm{OCB}}(g_Q)$, with normalization factor $\mathcal{N}$. The probability that all four electrons are postselected in the $|+\rangle$ state is

$$P = 1 - |g_Q|^2(2\langle a^{\dagger}a\rangle_{\rho} + 1) + O(|g_Q|^4). \tag{8}$$

Here, $\langle \ldots \rangle_{\rho}$ denotes the expectation value over the state ρ. The photon numbers before and after the OCB, $\langle a^{\dagger}a\rangle_{\rho}$ and $\langle a^{\dagger}a\rangle_{\rho'}$, are related as

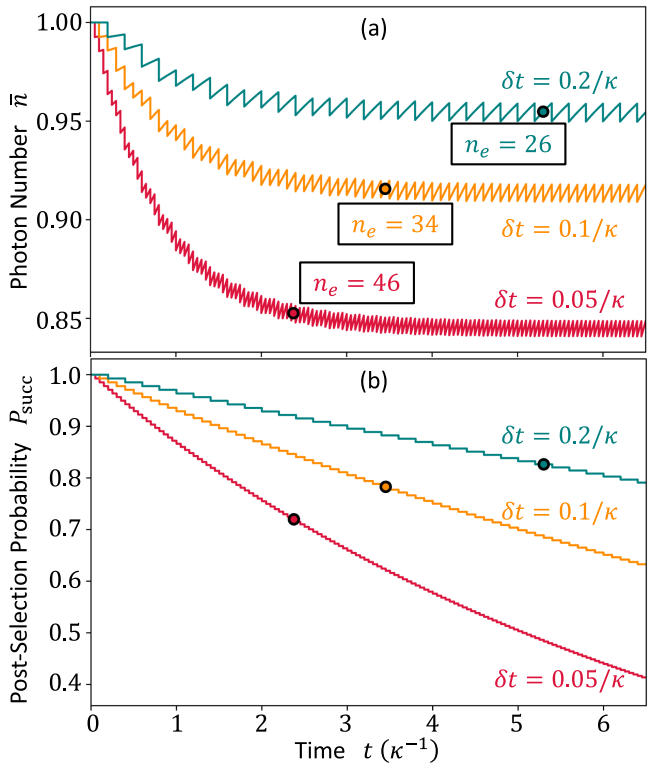

FIG. 2. Dynamics of the photon number and postselection probability. Time evolution of (a) the photon number $\bar{n}(t)$ and (b) the postselection probability $P_{\mathrm{succ}}(t)$. Time is normalized by the dissipation rate κ. The discontinuities correspond to applications of conditional displacement (CD) operations. Different time intervals δt between electrons are denoted by colors. Circle markers indicate the moments when the photon number stabilizes within a 1% accuracy (comparing adjacent maxima). The n_e values in the boxes indicate the number of electrons needed to achieve this stable regime. The parameters are $g_Q = 0.1$ and $\bar{n}^{(0)} = 1$.

$$\langle a^{\dagger}a\rangle_{\rho'} = \langle a^{\dagger}a\rangle_{\rho} - 2|g_Q|^2(\langle (a^{\dagger}a)^2\rangle_{\rho} - \langle a^{\dagger}a\rangle_{\rho}^2) + O(|g_Q|^4). \tag{9}$$

Thus, for small $|g_Q|$, the OCB reduces the photon number, except for Fock states $\rho = |m\rangle\langle m|$. An example of cooling a coherent state $\rho = |\alpha\rangle\langle\alpha|$ via D_{OCB} is given in Supplemental Material (Fig. S2) [60].

The OCB cooling mechanism can be visualized via the Wigner function. For real g_Q, the operators $D_+(\pm g_Q)$ produce effective squeezing along the x quadrature, while $D_+(\pm ig_Q)$ squeeze along p. This "bidirectional squeezing" narrows the Wigner distribution, reducing the photon number (see Supplemental Material for details [60]).

For a multimode cavity, the interaction in Eq. (5) occurs for all L modes with parameters $g_Q^{(l)}$, $l = 1, \ldots, L$: $CD = CD(g_Q^{(1)}) \otimes \ldots \otimes CD(g_Q^{(L)})$. Thus, each mode is cooled independently, with the efficiency set by its g_Q. Creating

the full OCB cycle for each mode requires the interaction phase control, e.g., for creating $CD(ig_Q)$. It can be done by setting the electron arrival time, which must be synchronized for different modes. Advances in microwave cavity engineering enable the selective suppression of all but a single mode [61,62]. Additional suppression is possible by controlling the electron position and velocity, relying on the phase matching [7,8]. These methods allow isolating the dynamics of the dominant mode with the largest $|g_Q|$, which we analyze below.

For an initial thermal state with the photon number $\bar{n}^{(0)}$, Eqs. (8) and (9) yield the photon number and the postselection probability after one OCB,

$$\bar{n}^{(1)} \approx \bar{n}^{(0)}\left(1 - 2|g_Q|^2(\bar{n}^{(0)} + 1)\right), \tag{10}$$

$$P^{(1)} \approx 1 - |g_Q|^2\left(2\bar{n}^{(0)} + 1\right). \tag{11}$$

The choice of interaction parameter g_Q and number of cooling cycles k involves a trade-off between the desired cooling efficiency and the acceptable probability threshold (see also Eqs. (S12) and (S13) in Supplemental Material [60]). Figure 1(c) shows gradual photon number decrease with more cooling operations. Figures 1(d1)–1(d3) show the Wigner functions of the states (c1)–(c3), respectively.

The key question is how efficient the approach is when $\kappa \neq 0$, i.e., when the cavity interacts with the bath. To address this, we model the sequential application of CD operators with time interval δt, while the system evolves under Eq. (3). We simulate this process [63] using the QuTiP package [64] and present the results in Fig. 2.

Figure 2(a) presents the evolution of $\bar{n}(t)$—the number of thermal photons at time t. It shows a sawtooth pattern: jumps correspond to CD operators (assuming instantaneous electron-cavity interaction), while the gradual rise between them arises from thermalization. After several cooling cycles, stable regime is reached, when the CD-induced cooling balances the heating. We define the stable regime to begin when the adjacent maxima differ by less than 1% (indicated by circle markers) and denote the corresponding photon number as $\bar{n}_\mathrm{f}$. The number of electrons n_e needed to reach this regime, depends on g_Q, δt, and the $\bar{n}(t)$ accuracy threshold (1%). The values of n_e are shown in the boxes in Fig. 2(a). After achieving the stable regime, further cooling requires decreasing δt or varying g_Q. Our findings show that the stable state closely approximates thermal state with photon number $\bar{n}_\mathrm{f}$, reaching fidelity of 99% or higher. The oscillation magnitude of $\bar{n}(t)$ at the stable regime can be estimated as $\delta\bar{n} \approx \kappa\delta t(n_\mathrm{b} - \bar{n}_\mathrm{f})$ (see Supplemental Material [60]).

Figure 2(b) shows the time evolution of the successful postselection probability $P_\mathrm{succ}(t)$—the probability that *all* electrons up to time t are measured in the $|+\rangle$ state. Each CD application is followed by a postselection, causing a

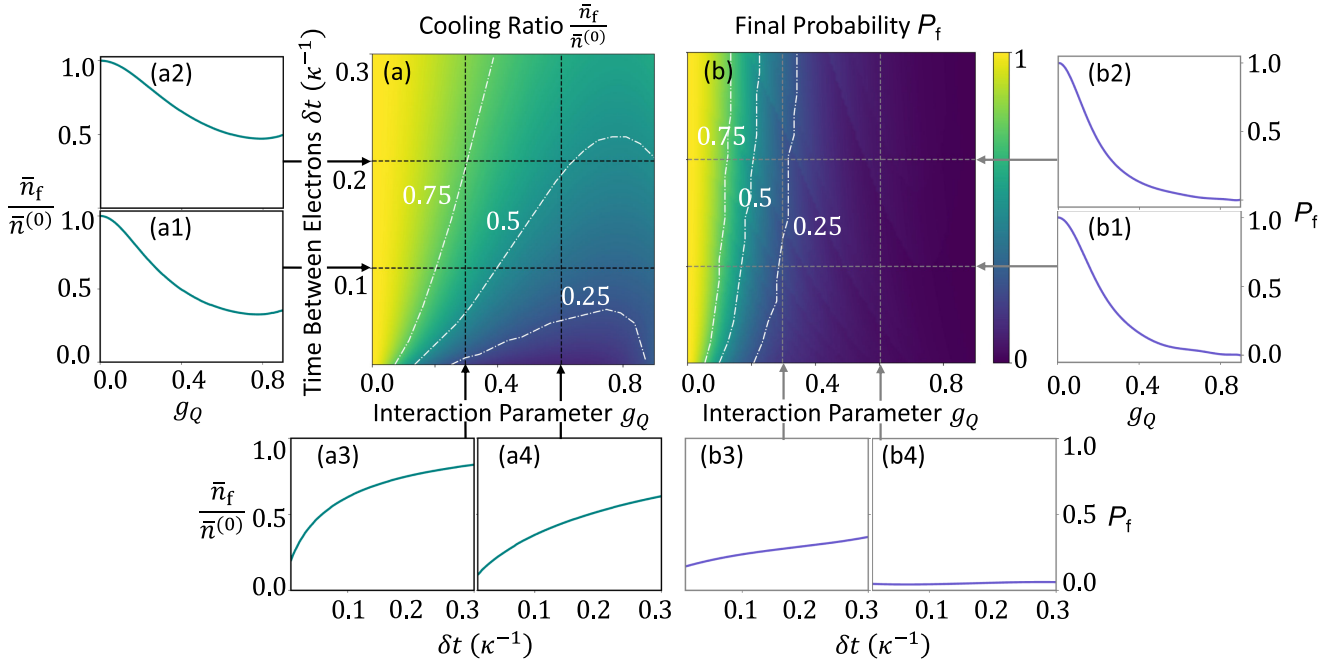

FIG. 3. Cooling efficiency and success probability as functions of the interaction parameter and electron-electron time interval. The heat maps present the ratio between the final and initial thermal photon numbers $\bar{n}_\mathrm{f}/\bar{n}^{(0)}$ (a) and the postselection probability P_f (b), both as a function of g_Q (horizontal) and δt (vertical). White dashed curves highlight contours with specific values. Slices of the heat map are presented for fixed time intervals $\delta t = (0.1/\kappa)$ (a1),(b1) and $\delta t = (0.2/\kappa)$ (a2),(b2), and for fixed interaction constants $g_Q = 0.3$ (a3),(b3) and $g_Q = 0.6$ (a4),(b4).

drop in probability. P_f denotes $P_{succ}(t)$ at the onset of the stable regime (circle markers). Its value is sensitive to the photon number accuracy threshold and increases when the requirement for $\bar{n}$ is less strict.

Figure 3 shows the cooling performance: the final-to-initial photon number ratio $\bar{n}_f/\bar{n}^{(0)}$ [Fig. 3(a)] and the final postselection probability P_f [Fig. 3(b)] as functions of g_Q and δt. White dashed lines indicate specific ratio and probability values, labeled on the plots. Auxiliary subplots show slices of the heat maps for fixed δt [Figs. 3(a1), 3(a2), 3(b1), and 3(b2)] and g_Q [Figs. 3(a3), 3(a4), 3(b3), and 3(b4)]. The heat maps show that the most effective cooling occurs at $g_Q \sim 0.6$ and $\kappa\delta t \ll 0.1$, resulting in a tenfold photon-number reduction but with success probabilities below 5%. More moderate cooling, e.g., twofold photon-number reduction, can be achieved with probabilities above 25%. It can be realized with $n_e = 40$ cooling electrons.

Discussion—The results underscore a trade-off between cooling efficiency and postselection probability. Stronger interactions and shorter electron intervals enhance cooling but reduce probability, so practical implementation must balance these factors. For a 20 GHz cavity, reducing the photon number from 1 to 0.5, attainable with 25% probability, corresponds to a temperature drop from 1.4 to 0.9 K. The former is achievable via liquid-helium precooling [65]; the latter is desirable for free-electron quantum optics experiments [23], though still above the millikelvin regime relevant to some quantum electron microscopy proposals [66–68]. Stronger cooling is possible with our protocol, albeit at lower success probabilities.

The experimental realization of cavity cooling with free electrons requires several demonstrated advances not yet combined in a single setup. Transverse coherence for electron holography reaches tens of microns [69], sufficient for microwave cavity scales. Beam splitter fidelity can exceed 50% [70], enabling effective cooling, with further improvements underway [71]. Precise electron arrival-time control is also essential: GHz-THz cavities require subcycle synchronization, attainable with laser-driven and cavity-controlled microscopes [72,73]. Attosecond-scale control has been demonstrated [5,74,75], far exceeding our requirements. The electron flux must surpass the thermal dissipation rate; present ultrafast transmission electron microscopes provide sufficient currents, especially when combined with high-Q cavities, where superconducting resonators reach millisecond photon lifetimes. For example, a 10-ms photon lifetime corresponds to $Q \sim 7 \times 10^8$ at 10 GHz [61]. For electron arrival intervals $\delta t \sim 0.1$ μs [76], twofold cooling occurs within ∼4 μs, well below the photon lifetime. With a 25% success probability, the effective rate is then $\sim 6.2 \times 10^4$ cooling events per second.

A promising application of this cooling technique is suppressing thermal noise in microwave cavities and detectors [77], relevant to quantum electron microscopy [66–68,78] and dark-matter searches [79,80]. An analog applies to optical cavities, advancing quantum optics toward novel light sources. More broadly, our which-path scheme extends to other oscillator systems, including phonons and polaritons in solids [44,45], and vibrational or rotational modes in molecules [46]. The universality stems from the common interaction Hamiltonian, as revealed by electron-energy loss spectroscopy, where these excitations imprint similarly on the electron spectrum [81,82]. The concept may further extend to other energetic probes, such as x-rays [47] or neutrons [48], which we leave for future investigation.

Acknowledgments—We acknowledge Qinghui Yan and Ron Ruimy for valuable discussions and early contributions to this work. This research was partially supported under the Flagship research project QUBIT by the Helen Diller Quantum Center at the Technion. This project was also funded in part by the Gordon and Betty Moore Foundation, through Grant No. GBMF11473 to Professor Ido Kaminer, and by the European Union—ERC COG, QinPINEM, Project No. 101125662.

Data availability—The data that support the findings of this article are openly available [63].

[1] B. Barwick, D. J. Flannigan, and A. H. Zewail, Nature (London) **462**, 902 (2009).
[2] F. J. García de Abajo, Rev. Mod. Phys. **82**, 209 (2010).
[3] S. T. Park, M. Lin, and A. H. Zewail, New J. Phys. **12**, 123028 (2010).
[4] A. Feist, K. E. Echternkamp, J. Schauss, S. V. Yalunin, S. Schäfer, and C. Ropers, Nature (London) **521**, 200 (2015).
[5] K. E. Priebe, C. Rathje, S. V. Yalunin, T. Hohage, A. Feist, S. Schäfer, and C. Ropers, Nat. Photonics **11**, 793 (2017).
[6] K. Wang, R. Dahan, M. Shentcis, Y. Kauffmann, A. Ben Hayun, O. Reinhardt, S. Tsesses, and I. Kaminer, Nature (London) **582**, 50 (2020).
[7] O. Kfir, H. Lourenço-Martins, G. Storeck, M. Sivis, T. R. Harvey, T. J. Kippenberg, A. Feist, and C. Ropers, Nature (London) **582**, 46 (2020).
[8] R. Dahan, S. Nehemia, M. Shentcis, O. Reinhardt, Y. Adiv, X. Shi, O. Be'er, M. H. Lynch, Y. Kurman, K. Wang *et al.*, Nat. Phys. **16**, 1123 (2020).
[9] K. E. Cahill and R. J. Glauber, Phys. Rev. **177**, 1882 (1969).
[10] O. Kfir, Phys. Rev. Lett. **123**, 103602 (2019).
[11] R. Dahan, A. Gorlach, U. Haeusler, A. Karnieli, O. Eyal, P. Yousefi, M. Segev, A. Arie, G. Eisenstein, P. Hommelhoff *et al.*, Science **373**, eabj7128 (2021).
[12] A. Gorlach, S. Malka, A. Karnieli, R. Dahan, E. Cohen, A. Pe'er, and I. Kaminer, Phys. Rev. Lett. **133**, 250801 (2024).
[13] R. Dahan, G. Baranes, A. Gorlach, R. Ruimy, N. Rivera, and I. Kaminer, Phys. Rev. X **13**, 031001 (2023).
[14] M. O. Scully and M. S. Zubairy, *Quantum Optics* (Cambridge University Press, Cambridge, England, 1997).
[15] P. T. Cochrane, G. J. Milburn, and W. J. Munro, Phys. Rev. A **59**, 2631 (1999).

[16] D. Gottesman, A. Kitaev, and J. Preskill, Phys. Rev. A **64**, 012310 (2001).
[17] B. M. Terhal, J. Conrad, and C. Vuillot, Quantum Sci. Technol. **5**, 043001 (2020).
[18] A. L. Grimsmo and S. Puri, PRX Quantum **2**, 020101 (2021).
[19] J. Hastrup and U. L. Andersen, Phys. Rev. Lett. **128**, 170503 (2022).
[20] B. De Neeve, T.-L. Nguyen, T. Behrle, and J. P. Home, Nat. Phys. **18**, 296 (2022).
[21] V. D. Giulio, M. Kociak, and F. J. G. de Abajo, Optica **6**, 1524 (2019).
[22] J.-W. Henke, A. S. Raja, A. Feist, G. Huang, G. Arend, Y. Yang, F. J. Kappert, R. N. Wang, M. Möller, J. Pan *et al.*, Nature (London) **600**, 653 (2021).
[23] R. Ruimy, A. Karnieli, and I. Kaminer, Nat. Phys. **21**, 193 (2025).
[24] R. Ruimy, A. Gorlach, G. Baranes, and I. Kaminer, Nano Lett. **23**, 779 (2023).
[25] R. Ruimy, O. Tziperman, A. Gorlach, K. Mølmer, and I. Kaminer, npj Quantum Inf. **10**, 121 (2024).
[26] V. Di Giulio and F. J. García de Abajo, Nanophotonics **11**, 4659 (2022).
[27] G. Baranes, S. Even-Haim, R. Ruimy, A. Gorlach, R. Dahan, A. A. Diringer, S. Hacohen-Gourgy, and I. Kaminer, Phys. Rev. Res. **5**, 043271 (2023).
[28] Y. Adiv, H. Hu, S. Tsesses, R. Dahan, K. Wang, Y. Kurman, A. Gorlach, H. Chen, X. Lin, G. Bartal *et al.*, Phys. Rev. X **13**, 011002 (2023).
[29] G. Huang, N. J. Engelsen, O. Kfir, C. Ropers, and T. J. Kippenberg, PRX Quantum **4**, 020351 (2023).
[30] M. Bézard, I. Si Hadj Mohand, L. Ruggierio, A. Le Roux, Y. Auad, P. Baroux, L. H. G. Tizei, X. Checoury, and M. Kociak, ACS Nano **18**, 10417 (2024).
[31] A. Karnieli, C. Roques-Carmes, N. Rivera, and S. Fan, ACS Photonics **11**, 3401 (2024).
[32] Z. Zhao, Phys. Rev. Lett. **134**, 043804 (2025).
[33] Z. Xie, Z. Chen, H. Li, Q. Yan, H. Chen, X. Lin, I. Kaminer, O. D. Miller, and Y. Yang, Phys. Rev. Lett. **134**, 043803 (2025).
[34] A. Feist, G. Huang, G. Arend, Y. Yang, J.-W. Henke, A. S. Raja, F. J. Kappert, R. N. Wang, H. Lourenço-Martins, Z. Qiu *et al.*, Science **377**, 777 (2022).
[35] Q. Yan, R. Ruimy, A. Niedermayr, and I. Kaminer, in *CLEO: Fundamental Science* (Optica Publishing Group, San Jose, CA, 2023), p. FF3D.1, 10.1364/CLEO_FS.2023.FF3D.1.
[36] A. O. Caldeira and A. J. Leggett, Phys. Rev. Lett. **46**, 211 (1981).
[37] M. S. Kim and V. Bužek, Phys. Rev. A **46**, 4239 (1992).
[38] M. Kim and V. Bužek, J. Mod. Opt. **39**, 1609 (1992).
[39] B. J. Brown, D. Loss, J. K. Pachos, C. N. Self, and J. R. Wootton, Rev. Mod. Phys. **88**, 045005 (2016).
[40] R. Y. Teh, P. D. Drummond, and M. D. Reid, Phys. Rev. Res. **2**, 043387 (2020).
[41] C. Elouard, D. A. Herrera-Martí, M. Clusel, and A. Auffèves, npj Quantum Inf. **3**, 9 (2017).
[42] A. Eickbusch, V. Sivak, A. Z. Ding, S. S. Elder, S. R. Jha, J. Venkatraman, B. Royer, S. M. Girvin, R. J. Schoelkopf, and M. H. Devoret, Nat. Phys. **18**, 1464 (2022).
[43] P. Campagne-Ibarcq, A. Eickbusch, S. Touzard, E. Zalys-Geller, N. E. Frattini, V. V. Sivak, P. Reinhold, S. Puri, S. Shankar, R. J. Schoelkopf *et al.*, Nature (London) **584**, 368 (2020).
[44] T. Low, A. Chaves, J. D. Caldwell, A. Kumar, N. X. Fang, P. Avouris, T. F. Heinz, F. Guinea, L. Martin-Moreno, and F. Koppens, Nat. Mater. **16**, 182 (2017).
[45] N. Rivera and I. Kaminer, Nat. Rev. Phys. **2**, 538 (2020).
[46] W. Xiong, Acc. Chem. Res. **56**, 776 (2023).
[47] S. K. Sinha, J. Phys. Condens. Matter **13**, 7511 (2001).
[48] A. T. Boothroyd, *Principles of neutron scattering from condensed matter* (Oxford University Press, New York, 2020).
[49] L. D. Landau and E. M. Lifshitz, *Quantum Mechanics: Non-Relativistic Theory* (Elsevier, New York, 2013), Vol. 3.
[50] E. Wigner, Phys. Rev. **40**, 749 (1932).
[51] H. Y. Fan and L. Y. Hu, Mod. Phys. Lett. B **22**, 2435 (2008).
[52] H. Saito and H. Hyuga, J. Phys. Soc. Jpn. **65**, 1648 (1996).
[53] A. Serafini, S. D. Siena, F. Illuminati, and M. G. A. Paris, J. Opt. B **6**, S591 (2004).
[54] H. Le Jeannic, A. Cavaillès, K. Huang, R. Filip, and J. Laurat, Phys. Rev. Lett. **120**, 073603 (2018).
[55] T. Tanigaki, Y. Inada, S. Aizawa, T. Suzuki, H. S. Park, T. Matsuda, A. Taniyama, D. Shindo, and A. Tonomura, Appl. Phys. Lett. **101** (2012).
[56] M. A. Nielsen and I. L. Chuang, *Quantum Computation and Quantum Information* (Cambridge University Press, Cambridge, England, 2010).
[57] D. P. DiVincenzo, Phys. Rev. A **51**, 1015 (1995).
[58] S. Even-Haim, A. A. Diringer, R. Ruimy, G. Baranes, A. Gorlach, S. Hacohen-Gourgy, and I. Kaminer, in *Quantum 2.0* (Optica Publishing Group, San Jose, CA, 2023), pp. QTh4C–6, 10.1364/CLEO_FS.2023.FM3A.6.
[59] K. Jacobs, *Quantum Measurement Theory and Its Applications* (Cambridge University Press, Cambridge, England, 2014).
[60] See Supplemental Material at http://link.aps.org/supplemental/10.1103/fnhk-lknl for additional details on the cooling protocol and supporting calculations.
[61] M. Reagor, W. Pfaff, C. Axline, R. W. Heeres, N. Ofek, K. Sliwa, E. Holland, C. Wang, J. Blumoff, K. Chou *et al.*, Phys. Rev. B **94**, 014506 (2016).
[62] T. Brecht, W. Pfaff, C. Wang, Y. Chu, L. Frunzio, M. H. Devoret, and R. J. Schoelkopf, npj Quantum Inf. **2**, 16002 (2016).
[63] L. Stettiner, D. Maison, and S. Even-Haim, https://github.com/lironst1/cooling_microwave_cavity_code accessed: November 2024, 25.
[64] J. R. Johansson, P. D. Nation, and F. Nori, Comput. Phys. Commun. **183**, 1760 (2012).
[65] S. Asztalos, E. Daw, H. Peng, L. Rosenberg, C. Hagmann, D. Kinion, W. Stoeffl, K. van Bibber, P. Sikivie, N. Sullivan *et al.*, Phys. Rev. D **64**, 092003 (2001).
[66] H. Okamoto, Phys. Rev. A **85**, 043810 (2012).
[67] H. Okamoto and Y. Nagatani, Appl. Phys. Lett. **104** (2014).
[68] H. Okamoto, R. Firouzmandi, R. Miyamura, V. Sazgari, S. Okumura, S. Uchita, and I. I. Kaya, Micron **161**, 103330 (2022).
[69] S. Tsujino, J. Vac. Sci. Technol. B **40**, 030801 (2022).

[70] Y. Yang, C.-S. Kim, R. G. Hobbs, P. Kruit, and K. K. Berggren, Phys. Rev. A **98**, 043621 (2018).
[71] D. Roitman, R. Shiloh, P.-H. Lu, R. E. Dunin-Borkowski, and A. Arie, ACS Photonics **8**, 3394 (2021).
[72] L. Zhao, Z. Wang, C. Lu, R. Wang, C. Hu, P. Wang, J. Qi, T. Jiang, S. Liu, Z. Ma *et al.*, Phys. Rev. X **8**, 021061 (2018).
[73] S. Borrelli, T. C. H. de Raadt, S. B. van der Geer, P. H. A. Mutsaers, K. A. H. van Leeuwen, and O. J. Luiten, Phys. Rev. Lett. **132**, 115001 (2024).
[74] Y. Morimoto and P. Baum, Nat. Phys. **14**, 252 (2018).
[75] N. Schönenberger, A. Mittelbach, P. Yousefi, J. McNeur, U. Niedermayer, and P. Hommelhoff, Phys. Rev. Lett. **123**, 264803 (2019).
[76] A. Ryabov, J. W. Thurner, D. Nabben, M. V. Tsarev, and P. Baum, Sci. Adv. **6**, eabb1393 (2020).
[77] J. Gao, *The Physics of Superconducting Microwave Resonators* (California Institute of Technology, Pasadena, CA, 2008).
[78] S. A. Koppell, Y. Israel, A. J. Bowman, B. B. Klopfer, and M. A. Kasevich, Appl. Phys. Lett. **120** (2022).
[79] N. Du, N. Force, R. Khatiwada, E. Lentz, R. Ottens, L. J. Rosenberg, G. Rybka, G. Carosi, N. Woollett, D. Bowring *et al.* (ADMX Collaboration), Phys. Rev. Lett. **120**, 151301 (2018).
[80] G. Bertone and T. M. Tait, Nature (London) **562**, 51 (2018).
[81] F. S. Hage, R. J. Nicholls, J. R. Yates, D. G. McCulloch, T. C. Lovejoy, N. Dellby, O. L. Krivanek, K. Refson, and Q. M. Ramasse, Sci. Adv. **4**, eaar7495 (2018).
[82] A. Polman, M. Kociak, and F. J. García de Abajo, Nat. Mater. **18**, 1158 (2019).